Eng. Sci., 2021, **16**, 187–193

Engineered Science

DOI: https://dx.doi.org/10.30919/es8d559

High-Efficiency Directional Radiation via Slow Light Resonance of Modified Photonic Crystal Array

Guoyan Dong,[1,*] Shuhui Zheng,[1] Huanhuan Wang,[1] Qian Zhao[2,*] and Ji Zhou[3,*]

Abstract

Directional light manipulation plays an important role in the optical link and communication of nanotechnology and modern optics. In this work, we provide a practical solution for directional radiation based on drastic slow light resonance near the photonic band-edge. Unidirectional stretched oscillations in the modified resonator almost completely suppress both longitudinal reflected and leaky losses to guarantee transverse scatterings with high directivity. The scaling invariance and flexible tunability of photonic crystal enable it to operate with relaxed structural parameters from infrared to microwaves. Microwave experiments have demonstrated the energy transfer and directional radiation process, agreeing well with the theoretical results. The iconic advantages of high transfer efficiency > 90%, far better directivity gain, 3db splitting, and flexible tunability make photonic crystal (PhC)-resonators promising for advanced application in the wireless link, filtering, and sensing of micro-nano integrated circuits.

Keywords: Directional radiation; Photonic crystal; Slow light resonance; Transverse scattering; photonic band edge.
Received: 16 October 2021; Accepted: 29 October 2021.
Article type: Research article.

1. Introduction

Directional light manipulation becomes valuable in modern optics and nanotechnology for high-efficiency electromagnetic wave (EMW) propagation. Some relevant researches focused on Mie[1,2] resonances due to their low absorption losses with more advantages in precise and tunable manipulation of light propagation. Three-layer onion-like nanoparticles[3] were optimized to realize anisotropic elliptical side-scattering, and four multipoles of two dipoles and two quadrupoles were proposed in a high-index subwavelength particle to achieve transverse scattering.[4,5] But the scattering signal of an individual subwavelength particle is too weak to be detected, so the ordered or random arrays were integrated to enhance the signal.[6] Periodic arrays composed of high-index nanoparticles with transverse scattering patterns[7,8] were applied for beam control of zero reflection. However, the process of appropriately modulating the resonances from multiple dielectric particles superposing and interfering[9] is very complex to control the light in an ideal direction.

Owing to the fantastic properties to prevent or support EMW propagation with low dissipative loss, dielectric photonic crystal (PhC)-antennas exhibit high directivity in optical and microwave wavelengths. Most current reported works were based on the total reflection of photonic bandgap (PBG), planar defects,[10] or suppressing surface modes.[11] In the micro-nano scale, zero-index metamaterials[12] and double-zero PhC[13] also support directional scattering. But strict degeneracy constraints and iterative attempts make them rather time-consuming and inefficient. Photonic band engineering of flat dispersion curves was used to induce zero diffraction,[14] resulting in collimating surface emission. However, the impedance mismatch between the air and the PhC prevents truly realistic implementations. The degenerate band edge PhCs at the border of the first Brillouin zone (FBZ)[15,16] were proposed to emulate anisotropic media for direction radiation, but only appliable in the microwave or requiring the source placed in certain positions of a PhC array.[17] Therefore, high-efficiency and facile alternatives are necessary to be explored.

[1] *Center of Materials Science and Optoelectronics Engineering, School of Optoelectronics, University of Chinese Academy of Sciences, Beijing 100049, China.*
[2] *State Key Laboratory of Tribology, Department of Mechanical Engineering, Tsinghua University, Beijing, 100084, China.*
[3] *State Key Laboratory of New Ceramics and Fine Processing, School of Materials Science and Engineering, Tsinghua University, Beijing, 100084, China.*
**E-mail:* gydong@ucas.ac.cn (G. Dong),
zhaoqian@tsinghua.edu.cn (Q. Zhao),
zhouji@tsinghua.edu.cn (J. Zhou)

2. Theoretical principle

Complex propagation problems in PhC can be cast as the linear Hermitian differential equation. The lattice function $\varepsilon(r)$ determines the solutions of propagation modes, which has a close relationship with the parameters of lattice spacing a, permittivity ε, and cylinder radii r. For the square-lattice PhC composed of Si-cylinders of the radius r=180 nm as an example, we applied the plane-wave expansion method to calculate the band structure of transverse magnetic (TM) mode with electric-field E along with the cylinders. Fig. 1(a) depicts the Dirac-cone dispersion (dash lines) as a=891 nm and the band-edge dispersion (solid lines) as a=692 nm, respectively. By decreasing the lattice spacing gradually, a bandgap appears between the 4th and the 2nd, 3rd bands. Meanwhile, the band-edge profile evolves from the Dirac-cone V-shape to a smooth U-shape, as the 3D diagrams shown in Figs. 1(b) and (c). To avoid the disturbance from other bands, we chose the 4th band as our study object. Their equal frequency contours (EFCs) are projected to the bottoms, like circle colormaps dividing the ordinate frequency with isotropic wavevector k around the FBZ center Γ. Hence, the PhCs can be regarded as homogeneous isotropic media with the effective refractive index derived from $n_{\text{eff}}=k/k_0$, where k_0 represents wavevector in air.

Sufficiently high permittivity represents the great capacity for storing energy, and low permittivity means weak energy constrain.[18] The frequency-dependent n_{eff} dispersion relations for increasing r/a ratios are shown in Fig. 1(d), changing from the Dirac-cone linear dispersion (solid line) to the band-edge parabolic dispersions. All of them show much low effective indexes $n_{\text{eff}} \ll 1$ near the FBZ center. The high density of states (DOS) near the van Hove singularities[19] accompanying the PBGs can greatly enhance quantum interference effects,[20] with the vanishing group velocity v_g near the band edge. The group velocity can be expressed as $v_g=d\omega/dk$, and the DOS is inversely proportional to the v_g. In Fig. 1(e), the group velocity v_g (red lines) and corresponding DOS (black lines) of the Dirac cone dispersion (solid lines) show minimal fluctuations in the FBZ. As a contrast, the v_g and DOS of the band-edge dispersions drastically change near the FBZ center, with the DOS value increasing by more than two orders of magnitude. With the r/a ratio increasing from 0.235 (dot line) to 0.26 (dash line), the DOS peak not only greatly increases but also further broadens. The high local DOS and much low effective index make this PhC distinctive near the band edge.

Since abrupt changes of permittivity at the surfaces would excite EMW reflections, most object blocks are characterized by resonant frequency. For a generic rectangular dielectric resonator of effective index n_{eff} and side length L, the resonant frequency can be predicted by using the transcendental equation[21]:

$$k_y \tan\left(k_y \frac{W}{2}\right) = \sqrt{(1-n_{\text{eff}}^2)k_0^2 + k_y^2} = \sqrt{k_0^2 - k_x^2}, \quad (1)$$

Where,

$$k^2 = k_x^2 + k_y^2 = n_{eff}^2 k_0^2, \quad k_0 = \frac{2\pi}{\lambda_0}$$

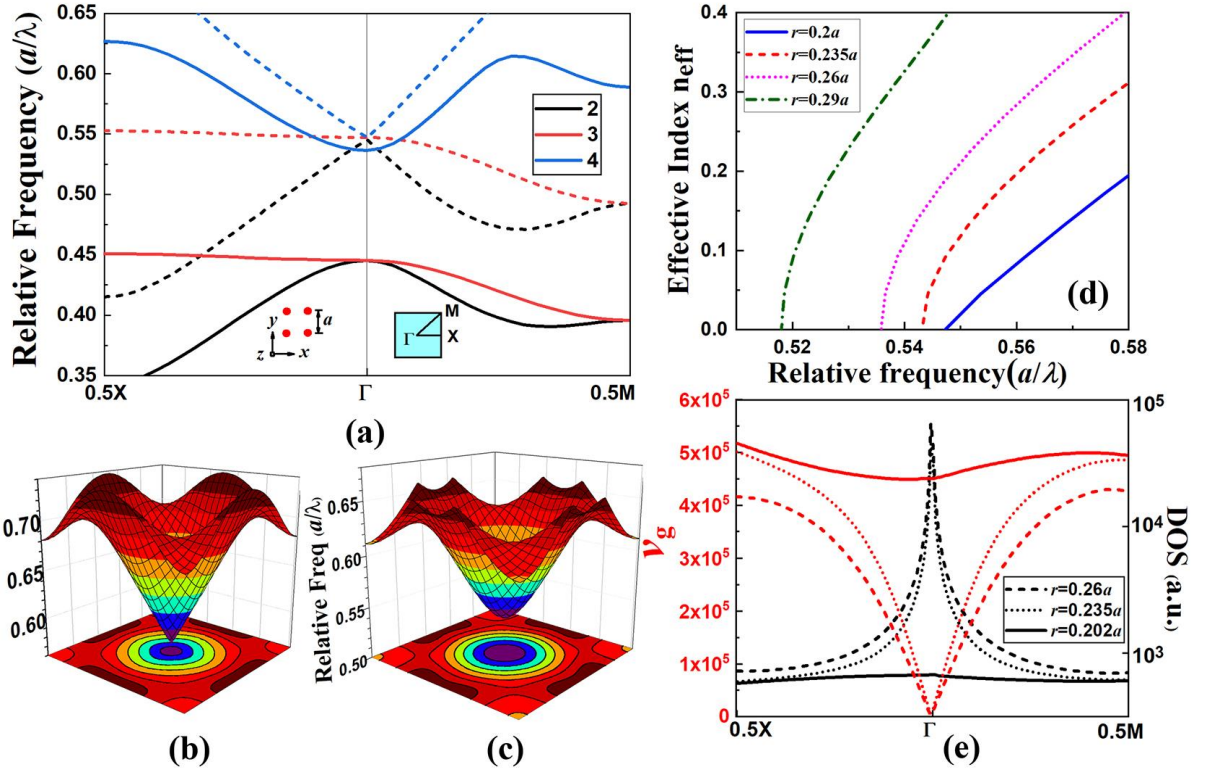

Fig. 1 (a) Band dispersion diagrams of PhCs composed of Si-nanocylinders of r=180 nm with different lattice spacings of a=891 nm (dash lines) and a=692 nm (solid lines). Corresponding 3D diagrams for (b) Dirac cone and (c) band-edge dispersions. (d) Frequency-dependent effective indices for various ratios r/a. (e) Group velocities v_g (red lines) inversed to DOSs (black lines) of Dirac Cone and two band-edge dispersions around the FBZ center Γ.

As a plane wave E_1 normally incidents into a square homogeneous media of $n_{eff} \ll 1$, the propagation wavelength would become much larger than that in air. Even if avoiding the impedance mismatches at the interfaces, it's still hard to excite intense resonance due to the weak capability of energy constraint for low index. Hence, we place a high reflector at the opposite exit surface along the incident x-direction to induce a reflected wave E_2 with an additional phase shift of π, arising from the half-wavelength loss at the reflector interface. The superposition of forwarding and backward waves can be expressed as

$$E = E_1(x,y) + E_2(-x,y) = 2A\sin(k_x x)\exp[i(k_y y - \omega t)] \quad (2)$$

The synthesis wave E becomes a y-directed traveling wave with the x-dependent amplitude of $2A\sin(k_x x)$. The resonant condition for the x-directed standing wave requires the side length $L=N\lambda/2$, N=1, 2, 3, …. so, $k_x=2\pi/\lambda = N\pi/L$. In the fundamental resonant mode, this operation can realize constant scattering phase profiles for beam vertical steering and beam splitting.

3. Calculation results and analysis

3.1 Directional radiation near band-edge

To verify the effect of the band-edge resonances, we construct two square-lattice PhC-resonator models composed of 9 × 9 and 20 × 20 Si-nanocylinders of the radius r = 180 nm and the lattice spacing a = 857 nm with the simulation software of Lumerical FDTD Solutions. Here, another PhC array with a bandgap covering the working frequency is utilized as the high reflector. The inset in Fig. 2(a) schematically displays the energy transfer process of a normally incident wave through the PhC-resonator for transverse scatterings. Fig. 2(a) shows the y-directed unilateral radiation spectra under the influences of a high reflector and the dimension of the band-edge PhC resonator. For the 9 × 9 case, the optimal resonant peak of transverse radiation spectra appears at the wavelength of 1535nm. Without the high reflector, the PhC array only excites a few weak resonances in the forms of small ups and downs in the transmission spectra. After adding a high reflector, a series of intense resonant peaks are detected, with the highest total transverse transmittance at the fundamental resonance. The x-directed E-field is completely restrained, and the confined energy can only emit along the y-directed transverse direction. For the larger 20 × 20 PhC-array, more resonant peaks can be excited with significant redshifts, meeting Eq. (2).

In addition to the augmented effect of resonance, Figs. 2(b)~(e) clarify the function of directional modulation by a high reflector. The internal E-fields at the 1st and 2nd resonant frequencies are stretched by the 20 × 20 PhC-array, propagating with divergent wavefronts. According to the continuous tangential components of wavevectors at the interfaces, the radiated beams or scatted wavevectors in Figs. 2(b) and 2(c) deflect away from the normal of the exit interfaces due to the low effective index n_{eff} different from 1 in air. After adding a high reflector, as shown in Figs. 2(d) and 2(e), x-directed standing wave oscillations are excited with the iconic features of constant phase, node line, and π inversion between the 1st and (e) the 2nd resonances. (f) Unilateral

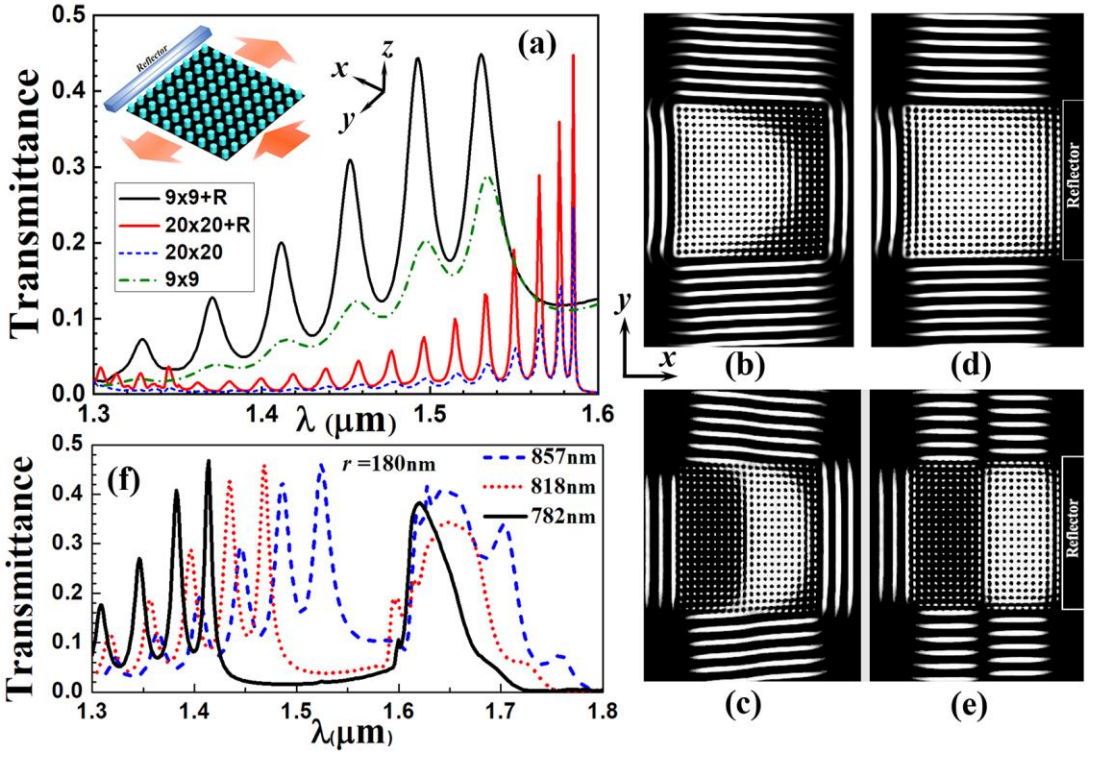

Fig. 2 (a) Unilateral y-directed radiation spectra for the 9 × 9 and 20 × 20 Si-PhC-arrays with (+R) and without a high reflector as r = 180nm and a = 860nm. E-fields without a reflector for the (b) 1st and (c) 2nd resonances. Modulated E-fields by a reflector for (d) the transmission spectra for the fixed r=180nm with different lattice spacings.

adjacent resonant regions. Directional traveling waves are emitted along the transverse *y*-direction, consistent with the theoretical prediction in Eq. (2). In the fundamental resonant mode of Fig. 2(d), the PhC-resonator acts like a perfect 3db splitter due to its symmetrical structure.

Note that the wavefront-modulation theory of zero-index metamaterials and the self-collimation techniques of photonic band engineering cannot explain these phenomena of directional transverse radiations here. Diffraction commonly arises from the dephasing between the plane-wave components and can be eliminated by a zero-amplitude field. The distance D between the PhC array and the reflector determines the phase difference between the reflected and leaky waves at the input interface. The specific conditions of destructive interference for simultaneous cancellation of both reflection and leakage losses can be satisfied at the input interface by exactly tuning the distance D, resulting in strong energy coupling and high efficiency of transverse scattering beyond 95%.

3.2 Performance Analysis with Varied Structural Parameters

As common dielectric resonator goes, possible resonance is associated with the structural parameters.[22] The lowest-order resonance often is the optimal mode, so our study focuses on the fundamental resonant mode. The band-edge effect can be applied independently on the PhC-resonator by varying the lattice spacing a or the cylinder radius r. Taking the above-mentioned 9 × 9 PhC array as an example, the variation of the lattice spacing leads to the change of resonator dimension and the dielectric filling ratio at the same time, which can be controlled by changing environment temperature. The unilateral transmission spectra of three cases are shown in Fig. 2(f). With the lattice spacing dropping, a bandgap appears gradually, and the resonant peaks blueshift. The detailed blueshift process of the fundamental resonant peak is illustrated in Fig. 3(a) with the full width at half maximum (FWHM) decreasing gradually. The impacts of lattice spacing a on the resonant wavelength λ (blue) and quality factor Q (black) are exhibited in Fig. 3(c). The linear relationships clarify this PhC-resonator is suitable for sensing measurements over a wide wavelength variation range. Since tightly confined field associated with optical resonant modes can be utilized to enhance nonlinear interactions,[23] the high Q factor covering the optical communication windows of 1310 nm and 1550nm signifies the PhC-resonator have prospects for optical field constraints, enhanced nonlinear effects, filters, isolators, *etc*.

For the fixed lattice spacing a = 800 nm, Fig. 3(b) depicts the redshift process of the fundamental resonant peak with the increasing cylinder radius r. As shown in Fig. 3(d), the Q-factor is more sensitive to the change of cylinder radius. Therefore, the PhC-resonator presents more signal adjustability, which is necessitated for high-performance single-mode lasers and other resonating systems. Inferred from the foregoing analyses, the dimension of the PhC-resonator plays a crucial role on the resonant wavelength, and the dielectric filling ratio becomes the dominant factor influencing the Q factor. Different from the incidental overlapping of the Fano resonance of an electric dipole and off-resonant quadrupoles[4] in the Mie nanoparticles, high-efficiency transverse scattering can be directly achieved by the PhC-resonators within a large variation range of structural parameters.

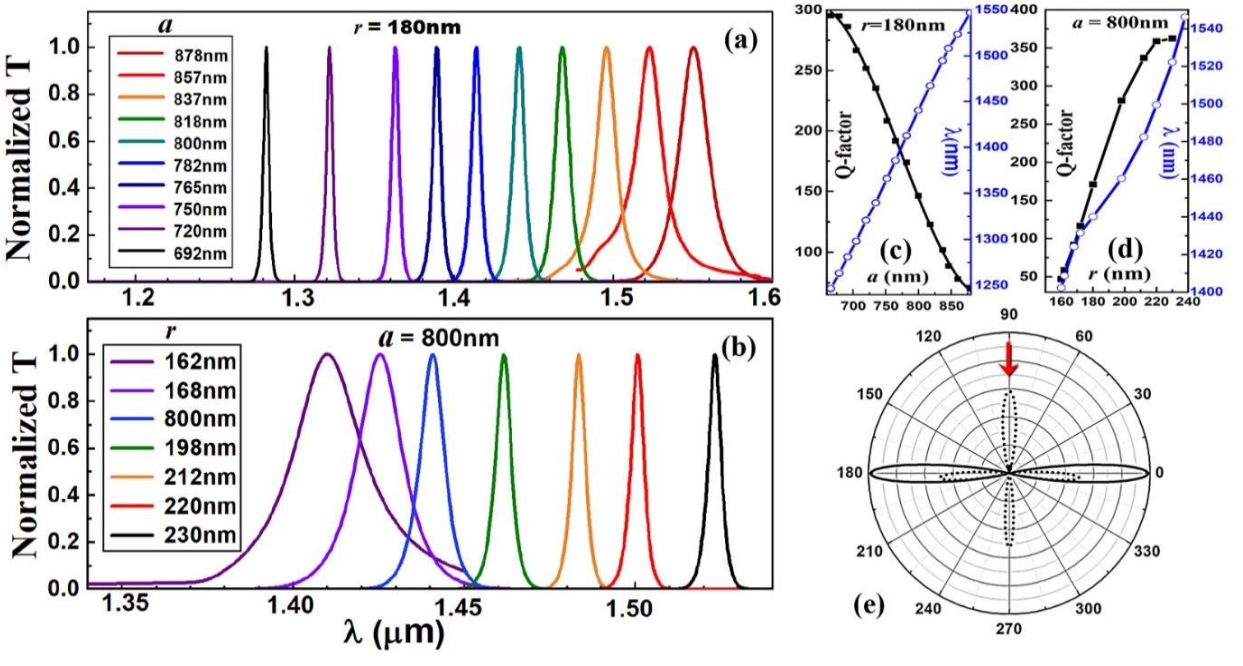

Fig. 3 Dependences of fundamental resonance on (a) the lattice spacing of a 9 × 9 Si-PhC resonators as r = 180nm, and on (b) the radius as a = 800 nm. Influences of (c) lattice spacing and (d) cylinder radius on Q factor and resonant wavelength λ_0. (e) Different far-field radiation patterns of the 9 × 9 PhC-array with (solid line) and without (dot line) a high reflector.

Traditional half-wavelength dipole antenna and Mie nanoantenna generally show the figure-8 shape radiation patterns in the far-field. Fig. 3(e) depicts the far-field radiation patterns of the 9 × 9 PhC-resonator, where the red arrow indicates the incident direction. The dot curves represent the radiation patterns of the PhC-array without a reflector. As can be seen, a small fraction of light energy is scattered transversely with a slight slant angle. The solid curves present the directional transverse emission patterns with the help of a high reflector. Nearly all incident energy concentrates in the symmetric main lobes of transverse directional radiations without visible side lobes, with the maximum directivity gain of 43-dBi. The directionality and radiation efficiency of this PhC-resonator is better than the previously reported PhC-based[24] and nanoparticle antennas.[25] Further researches indicate the larger PhC-array, the better directivity.

4. Experimental verification

To mimic the response properties of the nanocylinder array in infrared, we used the Al_2O_3 ceramic cylinders of r = 3.3 mm, h = 8 mm, ε_r = 10, and loss tangent tanδ ~ 10^{-4} to compose a 9 × 9 PhC-array model for validation in the microwave regime. As the schematic of the experimental setup shown in Fig. 4(a), a polished metallic bar of h = 8 mm is placed next to the exit interface of the PhC-array to form a 2D PhC-resonator. A microwave field mapping system is utilized to approximate a plane-wave excitation. The PhC-resonator sample is placed between two insulated conductors of the parallel plate. A polished metallic bar of h = 8 mm is placed next to the exit interface of the PhC-array to form a 2D PhC-resonator. A microwave field mapping system is utilized to approximate a plane-wave excitation. The PhC-resonator sample is placed between two insulated conductors of the parallel plate. A rectangular waveguide is connected to the transmitting port of a vector network analyzer (VNA) as the emitting probe, and a probe antenna is placed above the PhC-resonator to detect the E-field distributions. The radiation spectra can be detected by another rectangular waveguide connected to the VNA receiving port.

Measurements confirm the Dirac cone dispersion can be achieved at a = 15.5 mm, and the corresponding transmission spectrum (dash line) is shown in Fig. 4(e). When a=13.75 mm,

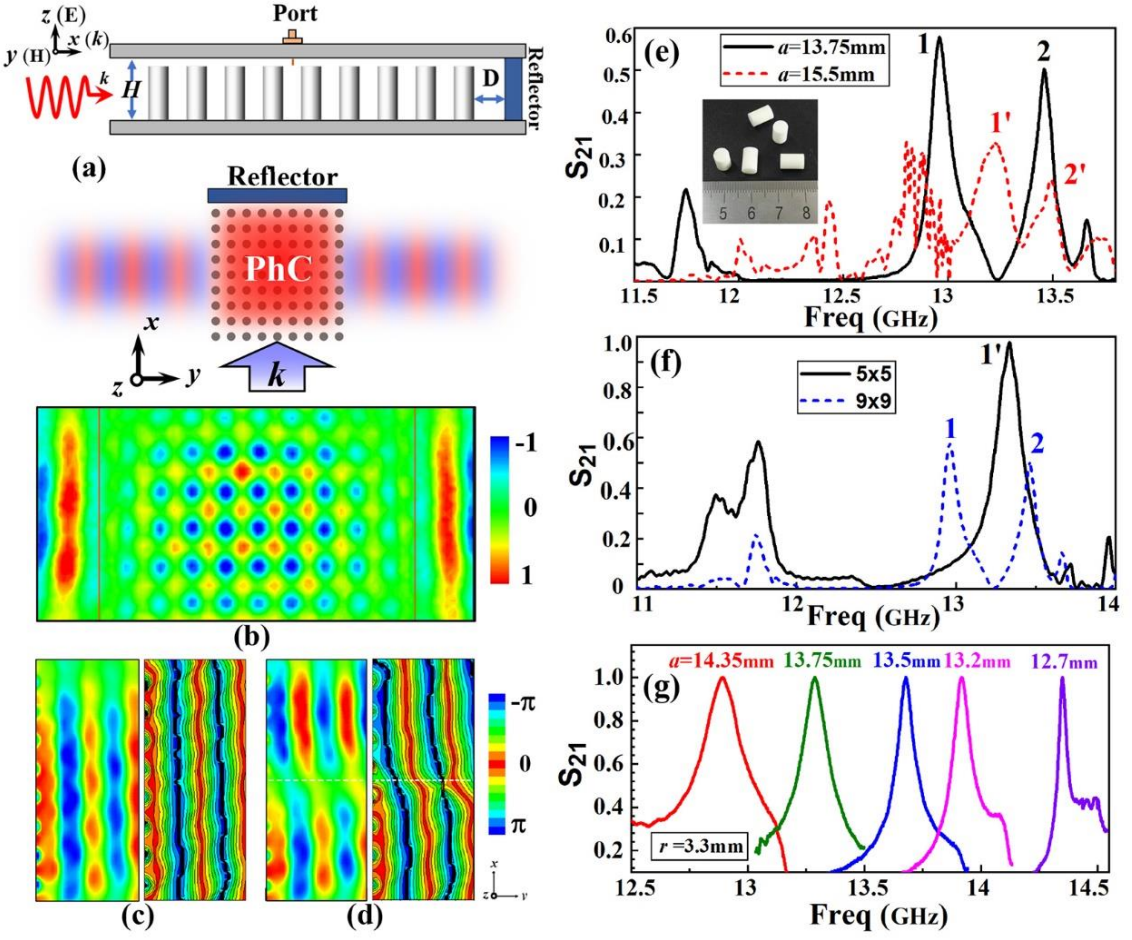

Fig. 4 Microwave experimental analog of 9 × 9 PhC-nanoantenna. (a) Schematic of the experimental setup with a PhC-resonator placed in a 2D E-field mapping system. (b) E-field distributions for the fundamental resonance and transverse external E-field and phase distributions for (c) the 1st and (d) the 2nd resonant modes as a = 13.75mm. (e) Detected transverse radiation spectra for band-edge (black solid line) and Dirc-cone dispersions (red dash line), with the orders of resonant peaks marked by the numbers. (f) Transmission spectra for 5 × 5 (solid line) and 9 × 9 (dash line) PhC-resonators. (g) Evolution of the fundamental resonant peak with the changing lattice spacing a.

a wide bandgap appears over the frequency scope of 11.8~12.7 GHz in the transmission spectrum (solid line). Compared to the former, quite higher resonant peaks with narrow FWHM appears near the right band edge, which demonstrates the band-edge effect of high DOS is a practical mechanism to strengthen resonances and enhance transfer efficiency. Fig. 4(b) gives the proof of *E*-field fundamental resonance inside the PhC-resonator with the constant phase distribution, accompanying strong external radiations with neat wavefronts parallel to the exit interfaces in Fig. 4(c). Especially explicit in Fig. 4(d), the obvious node line of the 2nd order standing-wave divides the internal field into two adjacent beams with the opposite phase of π. To further verify the influence of resonator dimension on the transverse radiation, as all else being equal, we detected the transmission spectra of the 5 × 5 and 9 × 9 PhC-resonators, respectively. In Fig. 4(f), a blueshift of the resonant peak with a particularly high transfer efficiency can be observed for the 5 × 5 PhC-resonator. It approves the resonant frequency is inversely associated with the resonator dimension and a small PhC-resonator just with a few periods can exhibit perfect transverse radiation near the band edge. The equivalent compact structure of the side length of several μm makes it easier to couple with the current microelectronic devices on a micro-nano scale. Fig. 4(g) validates the dependence of fundamental resonance on the lattice spacing by employing the already mentioned 9 × 9 PhC-resonators. The positive correlation between the lattice spacing and the resonant wavelength is completely compliant with the simulation results in Fig. 3(a).

5. Conclusion

We have proposed an efficient mechanism to realize high-efficiency directional radiation based on the band-edge resonance. We explained the principle of collimated transverse scattering and revealed the crucial role of the band-edge effect together with structural parameters for modulating the characteristics of transverse radiation. In sharp contrast to the harsh requirements of zero-index metamaterials and Mie particles, this band-edge PhC-resonator exhibits particular advantages of compact structure, high transfer efficiency, far better directivity, and flexible tunability. Finally, we demonstrated this scheme by microwave experiments in good agreement with the theoretical results. The predicted effects have application perspectives for optical antenna, wireless nano-link, filtering, and sensing.

Acknowledgments

This work is supported by the National Natural Science Foundation of China (11574311, 51872154, and 51788104), Joint Fund of Beijing University (111800S001), and the Beijing Municipal Science and Technology Commission (No. Z191100004819001).

Conflict of interest

There are no conflicts to declare.

Supporting information

Not applicable.

References

[1] Q. Zhao, Z. Xiao, F. Zhang, J. Ma, M. Qiao, Y. Meng, C. Lan, B. Li, J. Zhou, P. Zhang, N. Shen, T. Koschny, C. M. Soukoulis, *Adv. Mater.,* 2015, **27**, 6187-6194, doi : 10.1002/adma.201502298.

[2] Q. Zhao, J. Zhou, F. Zhang, D. Lippens, *Mater. Today,* 2009, **12**, 60-69, doi: 10.1016/S1369-7021(09)70318-9.

[3] J. Y. Lee, A. E. Miroshnichenko, R.-K. Lee, *Opt. Express,* 2018, **26**, 30393-30399, doi: 10.1364/OE.26.030393.

[4] H. K. Shamkhi, K. V. Baryshnikova, Andrey Sayanskiy, P. Kapitanova, P. D. Terekhov, P. Belov, A. Karabchevsky, A. B. Evlyukhin, Y. Kivshar, and A. S. Shalin, *Phys. Rev. Lett.,* 2019, **122**, 193905, doi: 10.1103/PhysRevLett.122.193905.

[5] K. V. Baryshnikova, D. A. Smirnova, B. S. Luk'yanchuk, Y. S. Kivshar, *Adv. Opt. Mater.,* 2019, **7**, 1801350, doi: 10.1002/adom.201801350.

[6] J. Xu, J. Cao, M. Guo, S. Yang, H. Yao, M. Lei, Y. Hao and K. Bi, *Adv. Compos. Hybrid Mater.,* 2021, **4**, 761-767, doi: 10.1007/s42114-021-00278-1.

[7] A. B. Evlyukhin, C. Reinhardt, A. Seidel, B. S. Luk'yanchuk, B. N. Chichkov, *Phys. Rev. B,* 2010, **82**, 045404, doi: 10.1103/PhysRevB.82.045404.

[8] K. Bi, Q Wang, J. Xu, L. Chen, C. Lan, M. Lei, *Adv. Opt. Mater.,* 2020, **9**, 2001474, doi: 10.1002/adom.202001474.

[9] K. Bi, D. Yang, J. Chen, Q. Wang, H. Wu, C. Lan and Y Yang *Photonics Res.,* 2019, **7**, 457-463, doi: 10.1364/PRJ.7.000457.

[10] H. Ammari, N. Béreux, E. Bonnetier, *Math. Method. Appl. Sci.*, 2001, **24**, 1021-1042, doi: 10.1002/mma.254.

[11] K. K. T. Hui Chen, and Andrew W. Poon, *Opt. Express,* 2006, **14**, 7368-7377, doi: 10.1364/OE.14.007368.

[12] T. Alam, M. T. Islam, M. Cho, *Sci. Rep.,* 2019, **9**, 3441, doi: 10.1038/s41598-019-40207-3.

[13] X. Huang, Y. Lai, Z. H. Hang, H. Zheng, C. T. Chan, *Nat. Mater.,* 2011, **10**, 582-586, doi: 10.1038/NMAT3030.

[14] N. Myoung, H. C. Park, A. Ramachandran, E. Lidorikis, J.-W. Ryu, *Sci. Rep.,* 2019, **9**, 2862, doi: 10.1038/s41598-019-39471-0.

[15] G. Mumcu, K. Sertel, J. L. Volakis, *IEEE Trans. Antennas Propag.,* 2009, **57**, 1618-1624, doi:10.1109/TAP.2009.2019874.

[16] S. Yarga, K. Sertel, J. L. Volakis, *IEEE Trans. Antennas Propag.,* 2009, **57**, 799-803, doi:10.1109/TAP.2009.2013451.

[17] S. Ceccuzzi, P. Baccarelli, C. Ponti, G. Schettini, in 2019 International Conference on Electromagnetics in Advanced Applications (ICEAA). (2019), pp. 0937-0940, doi: 10.1109/ICEAA.2019.8878961.

[18] R. K. Mongia, A. Ittipiboon, *IEEE Trans. Antennas Propag.,*

1997, **45**, 1348-1356, doi: 10.1109/8.623123.
[19] M. K. Moghaddam, R. Fleury, *Opt. Express,* 2019, **27**, 26229-26238, doi: 10.1364/OE.27.026229.
[20] S.-Y. Zhu, H. Chen, H. Huang, *Phys. Rev. Lett.,* 1997, **79**, 205-208, doi: 10.1103/PhysRevLett.79.205.
[21] A. Okaya, L. F. Barash, *Proc. IEEE Inst. Electr. Electron. Eng.,* 1962, **50**, 2081-2092, doi: 10.1109/JRPROC.1962.288245.
[22] S. Zheng, G. Dong, Q. Yang, H. Wang, J. Zhou, *Adv. Compos. Hybrid Mater.,* 2021, doi: 1007/s42114-021-00309-x.
[23] V. Zubyuk, L. Carletti, M. Shcherbakov, S. Kruk, *APL Materials,* 2021, **9**, 060701, doi: 10.1063/5.0048937.
[24] D. Headland, W. Withayachumnankul, R. Yamada, M. Fujita, T. Nagatsuma, *APL Photonics,* 2018, **3**, 126105, doi: 10.1063/1.5060631.
[25] N. Li,Y. Lai,S. H. Lam, H. Bai, L. Shao, J. Wang, *Adv. Opt. Mater.,* 2021, **9**, 2170002, doi: 10.1002/ADOM.202170002.

Author information

Guoyan Dong *received her Ph.D. from Shandong University in 2009. From 2011 to 2013, she worked as an assistant researcher in Tsinghua University. She is now an associate professor in University of Chinese Academy of Sciences. Her research group focuses on metamaterials, photonic crystals and nanophotonics.*

Shuhui Zheng *received her Ma. Eng. in optical engineering from University of Chinese Academy of Sciences, Beijing, China, in 2021. She is now an engineer in Communication Company. Her research interests include photonic crystals and metasurfaces.*

Huanhuan Wang *received her B.S. in applied physics from Heibei University, Baoding, China, in 2019. She is currently pursuing her master's degree in University of Chinese Academy of Sciences, Beijing, China. Her research interests include photonic crystals and metasurfaces.*

Qian Zhao *received his Ph.D. from Northwestern Polytechnical University in 2005. He is now an associate professor in Tsinghua University. His research focuses on metamaterials, metasurfaces and their applications.*

Ji Zhou *received his Ph.D. from Peking University in 1991. He is a professor of materials science in Tsinghua University, and selected as an academician of Chinese Academy of Engineering in 2017. His research focuses on metamaterials and information functional ceramics and devices.*